JOURNAL OF THERMOPHYSICS AND HEAT TRANSFER
Vol. 22, No. 4, October–December 2008

Analytical Model for Characterization of Loop Heat Pipes

Stéphane Launay,* Valérie Sartre,† and Jocelyn Bonjour‡
Université de Lyon, 69621 Lyon, France

DOI: 10.2514/1.37439

The present paper proposes general equations for predicting the steady-state behavior of a loop heat pipe, linking its operating temperature to various fluidic and geometrical parameters. The closed-form solutions determined for various loop-heat-pipe operating modes are deduced from the equations of a previously developed numerical model. This new approach of the loop-heat-pipe modeling facilitates the identification of the physical mechanisms that influence its operating behavior. In addition, the transition heat flux between variable and fixed conductance modes can also be estimated. This simplified model has been validated for each loop-heat-pipe operating mode for various geometries and operating conditions. The present model could be a useful tool for the design of loop heat pipes.

Nomenclature

A	=	cross-sectional area
c_p	=	specific heat
D	=	diameter
e	=	thickness
f	=	friction factor
g	=	gravitational acceleration
h	=	convective heat transfer coefficient
h_C	=	condensation heat transfer coefficient
K	=	overall heat transfer coefficient or permeability
k	=	thermal conductivity
L	=	length
l_v	=	latent heat of vaporization
$\dot{m}$	=	mass flow rate
P	=	pressure
Q	=	heat transfer rate
R	=	thermal resistance
R_p	=	pore radius
Re	=	Reynolds number
S	=	heat exchange surface area
T	=	temperature
ΔH	=	relative elevation
θ	=	wetting angle
μ	=	dynamic viscosity
ρ	=	density
σ	=	surface tension

Subscripts

A	=	ambient
C	=	condenser or condensation
E	=	evaporator
eff	=	effective
exp	=	experimental
i	=	input or inlet or inner
L	=	liquid line
l	=	liquid
max	=	maximum
model	=	simulated by the model
o	=	output or outlet or outer
R	=	reservoir
sink	=	heat sink
sat	=	saturation
sub	=	subcooled zone
t	=	total
trans	=	transition
V	=	vapor line
v	=	vapor
w	=	wick
wall	=	wall
2φ	=	two phase

Received 20 March 2008; accepted for publication 28 May 2008.

*Assistant Professor; currently Université de Provence, Institut Universitaire des Systèmes Thermiques Industriels, Unité Mixte de Recherche 6595, Centre National de la Recherche Scientifique, 5 rue Enrico Fermi, 13453 Marseille Cedex 13, France; stephane.launay@polytech.univ-mrs.fr.

†Associate Professor, Centre de Thermique de Lyon, Unité Mixte de Recherche 5008, Centre National de la Recherche Scientifique, de l'Institut National des Sciences Appliquées de Lyon et de l'Université Lyon1, Bâtiment Sadi Carnot, 20 Avenue Albert Einstein; valerie.sartre@insa-lyon.fr.

‡Professor, Centre de Thermique de Lyon, Unité Mixte de Recherche 5008, Centre National de la Recherche Scientifique, de l'Institut National des Sciences Appliquées de Lyon et de l'Université Lyon1, Bâtiment Sadi Carnot, 20 Avenue Albert Einstein; jocelyn.bonjour@insa-lyon.fr.

I. Introduction

LOOP heat pipes (LHP) are thermocapillary-driven two-phase heat transport systems that have already proved their efficiency in terms of thermal management of electronic devices under space or ground environmental conditions [1–4]. Compared with conventional heat pipes, LHPs have some additional advantages due to their particular design of capillary structure, allowing the transport of heat up to several meters at any orientation in the gravity field. The original concept of LHP allows a wide variety of different design embodiments of the evaporator/reservoir design or the flexibility in evaporator/condenser locations, which essentially extends the sphere of functional possibilities and practical applications of these systems [5].

Despite its theoretical operational robustness, LHP is a complex system that involves couplings of thermal and hydrodynamic physical mechanisms between its components (i.e., the evaporator, the compensation chamber, the condenser, or the liquid and vapor lines). Moreover, the LHP heat transfer characteristics are difficult to predict, as they are sensitive to numerous parameters [6]. Various LHP operating characteristics, which are usually analyzed in terms of a curve depicting the operating temperature (on ordinate) vs the heat input (on abscissa), have been experimentally observed [4,7–9]. The LHP operating curve may be U-shaped, flattened, or may increase linearly with the heat flux, depending on the heat sink and ambient temperatures and on the LHP thermal insulation (Fig. 1). Two main LHP operating modes have been described in the literature [10]: namely, the variable and fixed conductance modes. These modes are linked to the distribution of condenser heat transfer area: one part is used for condensation heat transfer, and the other one is for liquid subcooling. Indeed, the condensation phenomenon allows the

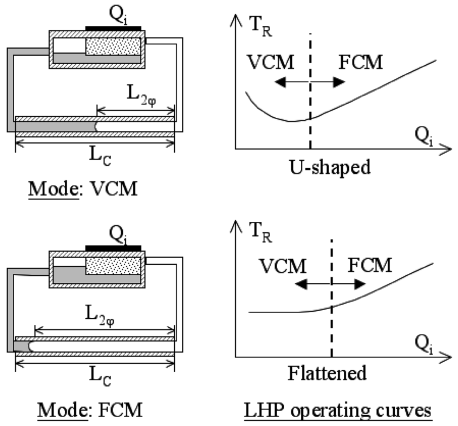

Fig. 1 Typical LHP operating curves.

transfer of a large part of the fluid enthalpy to the heat sink before returning back to the reservoir, and the liquid subcooling is necessary to compensate the heat leak from the evaporator to the reservoir. Here, the term heat leak refers to the fraction of the heat input that is not used for evaporating the fluid in the capillary structure and that is transferred (through the wick or through the material casing) to the fluid present in the reservoir. The decreasing part of the U-shaped curve and the flattened curve corresponds to the LHP variable conductance mode. In this mode, a fraction of the condenser heat transfer area is actually devoted to condensation, and the rest is devoted to liquid subcooling. The slope of the LHP characteristic curves (decreasing or almost flat) strongly depends on the amount of the evaporator/reservoir heat leak and on the heat exchange of the reservoir and the liquid line with the surroundings. Indeed, an increase of the heat input tends to reduce the liquid flow temperature variation along the liquid line due to the mass flow rate increase (proportional to the heat input) and, consequently, to reduce the LHP operating temperature. The minimum of the operating temperature appears when the liquid subcooling length in the condenser is no longer sufficient to cool down the liquid to the heat sink temperature at the condenser outlet. When the heat input further increases, most of the total condenser length is used for condensation heat transfer and the LHP starts to operate at a fixed conductance mode. Then the only way for the condenser to reject the additional heat is to increase the fluid saturation temperature, leading to an increase of the LHP temperature level. The increase of the temperature with the heat flux depends on the overall heat transfer coefficient between the condensing fluid and the heat sink, including the condenser design.

According to experimental results, it is difficult to predict the shape of the LHP operating curve, because the evaporator/reservoir heat leak is strongly influenced by the evaporator/reservoir design (wall materials and wick characteristics). U-shaped curves have been most often observed for metal capillary wicks, with ammonia as the working fluid [4,7] when the temperature difference between the sink and the ambient is large, whereas curves with flattened shapes have been usually observed for low-thermal-conductivity wicks with low-pressure working fluids such as methanol, ethanol, or acetone [8,9].

To predict the LHP characteristic curve or performance at steady state, various models have been developed [11–14]. Most of these models are based on the steady-state energy-conservation equations written for each component of the LHP. The accurate prediction of the LHP performances requires accurate modeling of all heat leaks and boundary conditions, especially for the compensation chamber and the liquid line. For more precise predictions of the LHP operating temperature, Hoang and Kaya [15] improved the two-phase pressure-drop calculation. Although such LHP models are acceptable for LHP thermohydraulic behavior predictions, they do not seem to be practical to use for the sake of a parameter sensitivity analysis. LHP models with analytical solutions are found in some research works. Maydanik et al. [16] developed an analytical model with a closed-form solution by using the energy balance in the compensation chamber and the pressure balance in the overall loop. For LHP with a metallic capillary wick and ammonia as the working fluid, the vapor temperature at the evaporator is correctly predicted for moderate heat flux, as long as the liquid temperature at the reservoir inlet is known. To specify key components of a basic LHP configuration, Furukawa [17] proposed a design code based on an analytical modeling. According to this code, the LHP can be numerically designed if its operating temperature is given as a specification.

The originality of the present study is to propose general simplified equations for predicting the LHP steady-state behavior, linking its operating temperature to various fluidic and geometrical parameters. The closed-form solutions determined for various LHP operating modes are deduced from a global numerical model, which is first presented in this paper. This new approach of the LHP modeling presents many advantages. First, the closed-form solutions facilitate the identification of the physical mechanisms which influence the variation of LHP operating temperature. In addition, the operating temperature and the thermal resistance may be predicted for most of the standard LHP designs. The transition heat flux between variable and fixed conductance modes may also be estimated from the present analytical model, which may be helpful for the condenser design. Moreover, the simplified analytical expressions are able to highlight those parameters, which have a significant influence on the LHP performance. This, it is believed, will assist researchers and thermal engineers when performing the system analysis during the design phase. Finally, these simplified expressions of the LHP operating temperature may be easily implemented in a complex system program into which electrical, thermal, or mechanical modules are coupled.

II. LHP Global Modeling

A. LHP Description and Model Assumptions

Figure 2 presents a functional schematic of the modeled LHP, which consists of a capillary pump, a reservoir (also called a compensation chamber), a condenser, and vapor and liquid transport lines. Whereas cylindrical-shaped capillary pumps hold higher working-fluid pressures, a flat evaporator is usually more convenient for electronic cooling because it better integrates with the component shapes. In the following, equations will be written for both of these configurations.

The steady-state model developed in this study is based on momentum- and energy-conservation equations and thermodynamic relationships. The following assumptions are adopted:

1) The reservoir contains both liquid and vapor phases (two-phase fluid) and the fluid is isothermal (the configuration for which the reservoir may be completely filled with liquid is not considered).

2) Part of the source heat flux, called *heat leak*, is transferred to the reservoir through the evaporator wall and through the porous wick.

3) All flows, laminar or turbulent, are considered incompressible.

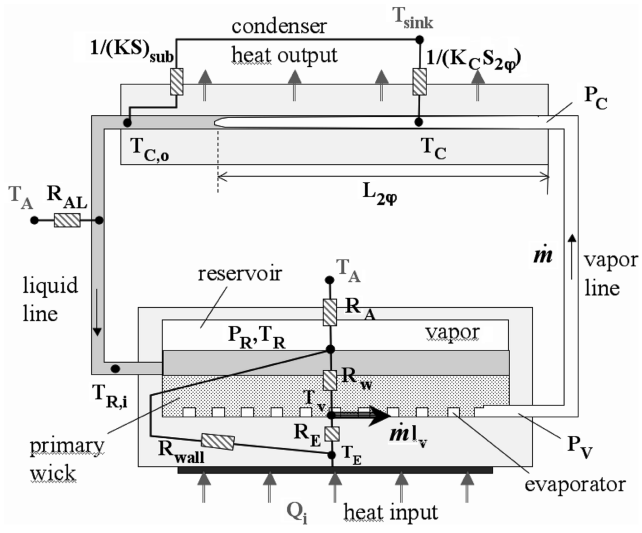

Fig. 2 LHP schematic and thermal resistance network.

4) Vapor temperature variations in the evaporator grooves and in the vapor line are neglected.

5) Liquid temperature variation due to heat exchange of the liquid line with the surroundings is taken into account.

6) Heat exchange between the reservoir and the surroundings is taken into account.

7) The desuperheating length in the condenser is neglected.

8) The phase change process in the condenser is isobaric.

9) Fluid thermophysical properties vary with the local temperature.

The originality of our model compared with Kaya et al.'s [12,13] and Hamdan et al.'s [14] model is the possibility to simulate various LHP evaporator geometries of cylindrical or flat disk shapes and to take into account the conductive heat transfer through the wall between the heat source and the reservoir. This heat leak can be dominant 1) in miniature LHPs for which the reservoir is located close to the evaporator, 2) in the case of high evaporator wall thermal conductivity having a great thickness compared with the other dimensions, and 3) in the case of poor wick thermal conductivity.

B. Energy Balance on Each LHP Component

The energy balance at the evaporator expresses that a part of the heat input Q_i is transferred to the reservoir by conduction through the evaporator wall and another part is transferred to the liquid–vapor interface at the wick level:

$$Q_i = \frac{T_E - T_R}{R_{\text{wall}}} + \frac{T_E - T_v}{R_E} \tag{1}$$

where R_E is the thermal resistance between the heat source to the vaporization interface at the porous wick surface, and R_{wall} is the conductive thermal resistance through the evaporator wall. The heat transferred to the liquid–vapor interface includes latent and sensible heats, plus conduction to the reservoir through the primary wick [14] (the heat flux is calculated at the internal diameter of the primary wick):

$$\frac{T_E - T_V}{R_E} = \dot{m} l_v + \dot{m} c_p (T_v - T_R) + \frac{T_V - T_R}{R_W} \tag{2}$$

where R_w represents the conductive thermal resistance inside the primary wick aided by convection in working fluid saturating the wick [14].

For a flat evaporator:

$$R_w = \frac{\exp\left(\dfrac{\dot{m} c_{p,l}}{k_{\text{eff}} A} e_w\right) - 1}{\dot{m} c_{p,l}} \tag{3}$$

For a cylindrical evaporator:

$$R_w = \frac{\exp\left(\dfrac{\dot{m} c_{p,l}}{2\pi k_{\text{eff}} L_w} \ell_n \dfrac{D_{w,o}}{D_{w,i}}\right) - 1}{\dot{m} c_{p,l}} \tag{4}$$

Relationships for the effective wick thermal conductivity k_{eff} were given by Mo et al. [18], depending on the thermophysical properties of the porous wick. In the reservoir, the heat leaking by conduction through the wall and by convective–conductive heat transfer through the wick is balanced by the reservoir heat exchange with the ambient and the returning-liquid subcooling at the reservoir inlet:

$$\dot{m} c_{p,l} (T_R - T_{Ri}) = \frac{T_E - T_R}{R_{\text{wall}}} + \frac{T_v - T_R}{R_w} - \frac{T_R - T_A}{R_A} \tag{5}$$

At the condenser, the energy balance is

$$Q_o = \dot{m} l_v + \dot{m} c_{p,l} (T_C - T_{Co}) \tag{6}$$

and

$$\dot{m} l_v = \frac{\pi L_{2\varphi}}{1/h_C D_{C,i} + 1/h_{\text{sink}} D_{C,o}} (T_C - T_{\text{sink}}) \tag{7}$$

where h_C is the condensation heat transfer coefficient, which depends on the two-phase flow regimes (e.g., stratified, annular, etc.). In Fig. 1, the term

$$\frac{\pi L_{2\varphi}}{1/h_C D_{C,i} + 1/h_{\text{sink}} D_{C,o}}$$

is denoted as $K_C S_{2\varphi}$ (i.e., the functional form of an overall heat transfer coefficient). Correlations for condensation heat transfer inside a smooth tube can be found in [19].

In the condenser zone dedicated to liquid subcooling, the liquid temperature T_{Co} at the condenser outlet is calculated considering a convective heat transfer with the heat sink:

$$T_{Co} = T_{\text{sink}} + (T_C - T_{\text{sink}}) \exp\left(-\frac{\pi D_{C,i} (L_C - L_{2\varphi})}{\dot{m} c_{p,l} (1/h_l + D_{C,i}/h_{\text{sink}} D_{C,o})}\right) \tag{8}$$

In Fig. 2, the term

$$\frac{\pi D_{C,i} (L_C - L_{2\varphi})}{1/h_l + D_{C,i}/h_{\text{sink}} D_{C,o}}$$

also appears as an overall heat transfer coefficient (namely, KS_{sub}). The convective heat transfer coefficient h_l between the liquid and the tube wall is calculated by considering a constant Nusselt number for laminar flow and using the Colburn correlation for turbulent flow [19]. The heat exchange between the liquid line and the ambient is expressed in a similar form to yield the liquid temperature T_{Ri} at the reservoir inlet:

$$T_{Ri} = T_A + (T_{Co} - T_A) \exp\left(-\frac{\pi D_{L,i} L_L}{\dot{m} c_{p,l} (1/h_l + D_{L,i}/h_A D_{L,o})}\right) \tag{9}$$

where h_A is the ambient heat transfer coefficient, which depends on the liquid-line boundary conditions (thermal insulation or natural convection heat transfer). Correlations for natural convection heat transfer around tubing can be found in [19].

C. Thermodynamic Equations

Because the LHP configuration for which the reservoir may be completely filled is not considered (case of excessive fill charge), there are three saturation states that are thermodynamically related. They are located in the evaporator grooves, in the reservoir, and in the condenser. Thus, the following conditions must be satisfied:

$$T_v - T_C = \left(\frac{\partial T}{\partial P}\right) \Delta P_v \tag{10}$$

$$T_C - T_R = \left(\frac{\partial T}{\partial P}\right) (\Delta P_l - \rho_l g \Delta H) \tag{11}$$

In Eq. (11), a positive elevation ΔH means that the condenser is placed above the evaporator, and a negative elevation means that the condenser is placed under the evaporator. The slope of the pressure–temperature saturation curve $\partial T/\partial P$ can be related to the thermophysical properties of the working fluid using the Clausius–Clapeyron equation:

$$\frac{\partial T}{\partial P} = \frac{T(1/\rho_v - 1/\rho_l)}{l_v} \tag{12}$$

The pressure drops ΔP_v and ΔP_l, due to the friction forces in the vapor and the liquid lines, depend on the fluid flow regime. They are calculated as follows:

$$\Delta P = \frac{f}{2\rho D} \left(\frac{\dot{m}}{A}\right)^2 L \tag{13}$$

Considering a hydraulically smooth tube wall of diameter D and length L, f is expressed by [19]

$$\begin{cases} f = 64/Re & \text{for laminar flow } (Re \leq 2000) \\ f = 0.316Re^{-0.25} & \text{for turbulent flow } (Re \geq 9510) \end{cases}$$

The friction factor for the transition flow between laminar and turbulent regimes is assumed to be constant in order to ensure the continuity in calculation of the pressure drops with the flow regimes (i.e., $f = 0.032$ for $2000 < Re < 9510$).

Equations (1–13) constitute the LHP global model under the form of a nonlinear system of equations. The numerical solution of this system leads to the prediction of the temperature and pressure distribution along the LHP and of the LHP performance as well. Nevertheless, due to physical phenomena couplings in a LHP, such modeling approach may be inappropriate to clearly capture the parameter sensitivity or to make discussions of the dominant physical phenomena governing the LHP operating steady-state performance.

D. Prediction of the LHP Capillary Limit

The model presented in the previous section can predict the maximum heat input corresponding to the capillary limit by considering the pressure balance of the fluid around the loop. For the LHP proper operation, the sum of the pressure drops due to frictional, inertial, and body forces must not exceed the maximum capillary pumping pressure created by the menisci in the wick:

$$\frac{2\sigma\cos\theta}{R_m} = \sum_j \Delta P_j(Q_i) \tag{14}$$

where R_m is the meniscus radius, θ is the wetting angle of the fluid in the porous wick, and ΔP_j corresponds to the pressure drop in the jth component of the LHP (vapor grooves in the evaporator, vapor line, condenser, liquid line, or porous wick). In Eq. (14), the inertia terms may be neglected, because they are largely dominated by the frictional pressure drops [12]. The frictional pressure drops in the LHP components are calculated using the fluid thermophysical properties at T_R and depend on the fluid mass flow rate (i.e., velocity) resulting from the heat input. Equation (14) can be rewritten as

$$\frac{2\sigma\cos\theta}{R_m} = P_v - P_R + \Delta P_w \tag{15}$$

where ΔP_w corresponds to the pressure drop inside the wick, calculated using the Darcy law:

$$\Delta P_w = \frac{\dot{m}\mu_l e_w}{K_w \rho_l A_w} \tag{16}$$

Equation (15) is used to determine the meniscus radius R_m, which is compared with the pore radius R_p. $R_m < R_p$ means that the wick is no longer able to provide a sufficient capillary pumping pressure to overcome the loop pressure drops. Consequently, the menisci will regress into the pores, bringing down the evaporator heat transfer coefficient. Then the operating temperature increases, which tends to reduce the overall pressure drop (linked to the variation of the fluid thermophysical properties function of the temperature), so that the pressure balance (14) is always satisfied.

III. LHP Analytical Model

A. Existing Closed-Form Solution of LHP Analytical Models

As mentioned, Maydanik et al. [16] developed an analytical model with a closed-form solution using the energy balance in the compensation chamber and the pressure balance in the overall loop. In their model, the heat leak from the evaporator to the reservoir was assumed to be a combination of heat and mass transfer conducted radially through a cylinder-shaped primary wick. The heat leak transferred to the reservoir through the evaporator casing and the heat exchange with ambient were neglected. Using Eq. (5), in which the first and third terms of the right-hand member were neglected, and replacing R_w by its expression [Eq. (4)], the following relationship was obtained:

$$T_R - T_{Ri} = \frac{T_v - T_R}{\left(\frac{D_{w,o}}{D_{w,i}}\right)^{\frac{\dot{m}c_{p,l}}{2\pi k_{\text{eff}} L_w}} - 1} \tag{17}$$

After rearrangement, this equation yields

$$T_v - T_{Ri} = \left(\frac{D_{w,o}}{D_{w,i}}\right)^{\frac{\dot{m}c_{p,l}}{2\pi k_{\text{eff}} L_w}} (T_R - T_{Ri}) \tag{18}$$

Assuming no temperature variation along the liquid line (low heat transfer between the liquid line and the ambient) and a heat load Q_i equal to the vaporization heat transfer (small heat leak compared with the vaporization heat flux), a simplified expression of the evaporator temperature T_v as a function of the heat load Q_i was given by

$$T_v = T_{Co} + (T_R - T_{Co})\left(\frac{D_{w,o}}{D_{w,i}}\right)^{\frac{Q_i c_{p,l}}{2\pi k_{\text{eff}} L_w l_v}} \tag{19}$$

Therefore, in Maydanik et al.'s [16] closed-form solution, predicting the vapor temperature requires the knowledge of the condenser outlet temperature T_{Co}.

B. Development of Closed-Form Solutions for the Various LHP Operating Modes

It is usually admitted in the literature that when the LHP operates below its operating limits, at least two distinct operating modes are likely to be observed. The LHP operates at variable conductance mode (VCM), which is achieved when T_{Co} is close to T_{sink}, when the portion of the area of the condenser in which liquid subcooling is taking place is large enough (if $S_{\text{sub}} \to \infty$, then $T_{Co} \to T_{\text{sink}}$). In this mode, two particular operating curve trends $T_R(Q)$ are described: namely, a U-shaped curve or a flattened curve. The temperature trend depends on the heat-flux distribution between the evaporator and the reservoir, on the heat exchange between the subcooled liquid in the liquid line and the surroundings, and on the heat exchange between the reservoir and the surroundings. It can be noted that specific mechanisms of heat transfer process may act, depending on whether the heat leak is transferred by conductive heat transfer through the wick aided by convection in working fluid saturating the wick or by conduction through the evaporator casing. The fixed conductance mode (FCM) is characterized by a quasi-linear increase of the LHP operating temperature with the heat flux. The temperature variation mainly depends on the condenser global heat exchange and is less sensitive to the heat leak distribution.

To predict most of the common LHP thermal behaviors and to simplify the analysis of the parameter sensitivity on the LHP performance depending on its boundary conditions, simplified equations for each LHP operating mode are presented in this section. These simplified equations are deduced from the nonlinear equation system developed previously in Sec. II.B. Because the dominant physical mechanisms governing the operating behavior of LHP during VCM and FCM are very different, two analytical expressions of T_R are proposed to describe the complete LHP operating curve. The total thermal resistance of the system R_t, which characterizes the LHP thermal performance, can be defined as a function of T_R as

$$R_t = \frac{T_E - T_{\text{sink}}}{Q_i} = \frac{T_E - T_R}{Q_i} + \frac{T_R - T_{\text{sink}}}{Q_i} \tag{20}$$

Assuming a small heat leak compared with the heat input Q_i, and $(T_v - T_R) \ll (T_R - T_{\text{sink}})$, R_t can be expressed as

$$R_t = R_E + \frac{T_R - T_{\text{sink}}}{Q_i} \tag{21}$$

1. *Development of a Closed-Form Solution in VCM*

The temperature difference between the reservoir and the heat sink can be shared into three terms:

$$T_R - T_{\text{sink}} = (T_R - T_{Ri}) + (T_{Ri} - T_{Co}) + (T_{Co} - T_{\text{sink}}) \quad (22)$$

The temperature difference $(T_{Co} - T_{\text{sink}})$ between the heat sink and the liquid at the condenser outlet can be neglected because the subcooled area in the condenser is large enough. In VCM, the term $T_R - T_{Ri}$ is deduced from the energy balance in the reservoir [Eq. (5)]:

$$T_R - T_{\text{Ri}} = \frac{1}{\dot{m} c_{p,l}} \left(\frac{T_E - T_v}{R_{\text{wall}}} + \frac{T_v - T_R}{R_{\text{wall}}} + \frac{T_v - T_R}{R_w} - \frac{T_R - T_A}{R_A} \right) \quad (23)$$

Because the heat leaks are usually small compared with the heat flux responsible for vaporization, then

$$Q_i \approx \dot{m} l_v \quad (24)$$

and the energy balance in the evaporator [Eq. (2)] yields

$$\dot{m} l_v \approx \frac{T_E - T_v}{R_E} \quad (25)$$

The combination between Eqs. (10–12) and (23–25) results in

$$T_R - T_{Ri} = \frac{R_E}{R_{\text{wall}}} \frac{l_v}{c_{p,l}} + \frac{1}{Q_i} \left[\frac{T_R}{\rho_v c_{p,l}} \left(\frac{1}{R_w} + \frac{1}{R_{\text{wall}}} \right) \times (\Delta P_v + \Delta P_l - \rho_l g \Delta H) - \frac{l_v}{c_{p,l} R_A} (T_R - T_A) \right] \quad (26)$$

Assuming $T_{Co} \approx T_{\text{sink}}$ in VCM, the temperature difference $(T_{Ri} - T_{Co})$ of Eq. (22), which depends on the heat exchanges between the liquid line and the ambient, is expressed using Eq. (9):

$$T_{Ri} - T_{Co} = (T_A - T_{\text{sink}}) \left[1 - \exp\left(- \frac{\pi D_L L_L K_L}{Q_i} \frac{l_v}{c_{p,l}} \right) \right] \quad (27)$$

where K_L is the overall heat transfer coefficient between the working fluid in the liquid line and the ambient.

Replacing the right terms of Eq. (22) by the expressions (26) and (27) yields

$$T_R - T_{\text{sink}} = \frac{R_E}{R_{\text{wall}}} \frac{l_v}{c_{p,l}} + \frac{1}{Q_i} \left[\frac{T_R}{\rho_v c_{p,l}} \left(\frac{1}{R_w} + \frac{1}{R_{\text{wall}}} \right) \times (\Delta P_v + \Delta P_l - \rho_l g \Delta H) - \frac{l_v}{c_{p,l} R_A} (T_R - T_A) \right] + (T_A - T_{\text{sink}}) \left[1 - \exp\left(- \frac{\pi D_L L_L K_L}{Q_i} \frac{l_v}{c_{p,l}} \right) \right] \quad (28)$$

Equation (28) can be rewritten as

$$T_R = \frac{T_{\text{sink}} + \frac{l_v}{c_{p,l}} \left[\frac{R_E}{R_{\text{wall}}} + \frac{T_A}{R_A Q_i} \right] + (T_A - T_{\text{sink}}) \left[1 - \exp\left(- \frac{\pi D_L L_L K_L}{Q_i} \frac{l_v}{c_{p,l}} \right) \right]}{1 - \frac{1}{Q_i} \left[\frac{1}{\rho_v c_{p,l}} \left(\frac{1}{R_w} + \frac{1}{R_{\text{wall}}} \right) (\Delta P_v + \Delta P_l - \rho_l g \Delta H) - \frac{l_v}{c_{p,l} R_A} \right]} \quad (29)$$

to yield the general closed-form solution of T_R in VCM.

A first-order approximation of the exponential function as $\exp(-x) 1 - x$ may be used with a relative uncertainty lower than 20% if $0 < x < 0.5$. Thus, if

$$Q_i > \frac{2\pi D_L L_L K_L l_v}{c_{p,l}}$$

then Eq. (27) may be simplified to

$$T_{Ri} - T_{Co} = (T_A - T_{\text{sink}}) \frac{\pi D_L L_L K_L l_v}{c_{p,l}} \frac{1}{Q_i} \quad (30)$$

Note that Eq. (30) is valid whatever the LHP operating mode, providing that the aforementioned condition is respected. Then Eq. (29) may be simplified to

$$T_R = \frac{T_{\text{sink}} + \frac{l_v}{c_{p,l}} \left[\frac{R_E}{R_{\text{wall}}} + \frac{1}{Q_i} \left(\frac{T_A}{R_A} + (T_A - T_{\text{sink}}) \pi D_L L_L K_L \right) \right]}{1 - \frac{1}{Q_i} \left[\frac{1}{\rho_v c_{p,l}} \left(\frac{1}{R_w} + \frac{1}{R_{\text{wall}}} \right) (\Delta P_v + \Delta P_l - \rho_l g \Delta H) - \frac{l_v}{c_{p,l} R_A} \right]} \quad (31)$$

where ΔP_v and ΔP_l can be expressed as a function of the fluid thermophysical properties and the LHP geometry using Eq. (13). Because ΔP_v and ΔP_l depend on Q_i^n (with $n > 0$), it can be deduced from Eq. (31) that the temperature decrease of the U-shaped curve $T_R(Q_i)$ is mainly due to heat exchanges of the liquid line and the reservoir with the ambient.

2. *Development of a Closed-Form Solution in FCM*

In fixed conductance mode, the numerical simulations [20] have shown that LHP heat transfer is governed by the condenser thermal resistance. Thus, the temperature variations within the working fluid are small compared with the difference between the condensation and heat sink temperatures:

$$(T_v - T_C) \ll (T_C - T_{\text{sink}}) \qquad (T_v - T_R) \ll (T_C - T_{\text{sink}})$$
$$(T_R - T_C) \ll (T_C - T_{\text{sink}})$$

As a result, $T_R - T_{\text{sink}}$ is deduced from Eq. (7):

$$T_R - T_{\text{sink}} \approx T_C - T_{\text{sink}} = \frac{\dot{m} l_v}{\pi D_C L_{2\varphi} K_C} \quad (32)$$

where D_C represents $D_{C,i}$ or $D_{C,o}$, depending on the surface area reference used in K_C.

In Eq. (32), the latent heat $\dot{m} l_v$ and the two-phase flow length $L_{2\varphi}$ have to be made explicit. With the previous assumptions, the reservoir energy balance [Eq. (2)] can be rewritten as follows:

$$\frac{T_E - T_v}{R_E} \approx \dot{m} l_v \quad (33)$$

where $T_E - T_v$ is determined using the evaporator wall energy balance [Eq. (1)]:

$$Q_i \approx (T_E - T_v) \left(\frac{1}{R_{\text{wall}}} + \frac{1}{R_E} \right) = \dot{m} l_v \left(1 + \frac{R_E}{R_{\text{wall}}} \right) \quad (34)$$

This equation expresses that the heat input is shared into two components: the latent heat and the heat leak. By comparing Eq. (34) with the condenser energy balance [Eq. (6)], it appears that the heat

leak is equal to the heat required to saturate the subcooled liquid. Considering a low variation of the fluid temperature in the subcooled zone, a simplified equation for this heat balance is used:

$$Q_i - \dot{m} l_v \approx \pi D_C (L_C - L_{2\varphi}) K_{\text{sub}} (T_C - T_{\text{sink}}) \tag{35}$$

where K_{sub} is the overall heat transfer coefficient between the working fluid and the heat sink. Combining Eqs. (32), (34), and (35) leads to the expression of the two-phase length:

$$L_{2\varphi} = \frac{L_C}{\dfrac{R_E}{R_{\text{wall}}}\dfrac{K_C}{K_{\text{sub}}} + 1} \tag{36}$$

Combining Eqs. (32), (34), and (36),

$$T_R = T_{\text{sink}} + \frac{Q_i}{\pi D_C L_C K_C} \frac{1 + \dfrac{R_E}{R_{\text{wall}}}\dfrac{K_C}{K_{\text{sub}}}}{1 + \dfrac{R_E}{R_{\text{wall}}}} \tag{37}$$

Equation (37) is the general closed-form solution of T_R in FCM.

3. Synthesis of the Model Closed-Form Solutions

The equations of the simplified steady-state thermohydraulic model are summarized in Table 1 for both LHP operating modes. Using these equations, the operating temperature of the system can be easily calculated as a function of the heat input. The equations of Table 1 are valid as long as $Q_i \leq Q_{\max}$, where $Q_{\max}$ is the maximum heat input corresponding to the LHP capillary limit. $Q_{\max}$ is thus the solution of the equation

$$\frac{2\sigma \cos\theta}{R_p} = \sum_j \Delta P_j (Q_{\max}) \tag{38}$$

IV. Analytical Model Validation and Results

The validation of the LHP analytical model has been performed by comparing the results of the analytical model and the numerical model for two LHP designs presented in the literature [8,21,22]. The main characteristics of the modeled LHP are presented in Table 2. These works have been selected for the validation procedure because the effect of several parameters on the LHP performance is explicitly shown, which provides useful information. These parameters are the working fluid, the evaporator shape, the wick characteristics (thermal conductivity, pore diameter, etc.), the heat sink temperature, and the LHP elevation.

For various reasons, some other thermal parameters such as the evaporator thermal resistance R_E or the heat transfer coefficients K_C, K_{sub}, and K_L are difficult to calculate. According to our literature review, no analytical model for the prediction of evaporation heat transfer coefficient in the capillary structures has yet been established. Moreover, because it is difficult to determine the evaporation-front position in the capillary wick due to complex coupled physical mechanisms, the evaporator heat transfer (evaporator thermal resistance R_E) is difficult to estimate. In addition, it also depends on the mechanical contact between the container and the wick and on the wettability of the liquid with the porous wick, which renders its estimation even more difficult. Indeed, a high-wetting fluid has a better ability to fill the porous medium and thus to reduce the thermal resistance between the container wall and the evaporation interface. Because such characteristics are not detailed in experimental studies, R_E has to be adjusted in the model in order to obtain a good agreement between experimental and model results. It must nevertheless be stated that R_E was numerically fixed for each working to a single value. For the LHP geometry of Boo and Chung [8], R_E was adjusted at the maximum thermal load, for which the evaporator temperature T_E is near 90°C, following the equation

$$R_E = \frac{T_E - T_v}{Q_i} = \frac{90 - T_v}{Q_{i_{\max}}} \tag{39}$$

Table 1 General closed-form analytical model for both modes of LHP steady-state operation

LHP modes	LHP operating temperature, K
VCM	$T_R = \dfrac{T_{\text{sink}} + \dfrac{l_v}{c_{p,l}}\left[\dfrac{R_E}{R_{\text{wall}}} + \dfrac{T_A}{R_A Q_i}\right] + (T_A - T_{\text{sink}})\left[1 - \exp\left(-\dfrac{\pi D_L L_L K_L}{Q_i}\dfrac{l_v}{c_{p,l}}\right)\right]}{1 - \dfrac{1}{Q_i}\left[\dfrac{1}{\rho_v c_{p,l}}\left(\dfrac{1}{R_w} + \dfrac{1}{R_{\text{wall}}}\right)(\Delta P_v + \Delta P_l - \rho_l g \Delta H) - \dfrac{l_v}{c_{p,l} R_A}\right]}$
FCM	$T_R = T_{\text{sink}} + \dfrac{Q_i}{\pi D_{C,i} L_C K_C} \dfrac{1 + \dfrac{R_E}{R_{\text{wall}}}\dfrac{K_C}{K_{\text{sub}}}}{1 + \dfrac{R_E}{R_{\text{wall}}}}$

Table 2 Geometry and thermal conditions of the LHPs used for the model validation

	LHP tested by Boo and Chung [8]	LHP tested by Chuang [21]
Working fluids	Methanol, acetone, ethanol	Ammonia
Relative elevation between condenser and evaporator	0	−10.2 to 10.2 cm
LHP casing material	Stainless steel	Aluminum (evaporator), stainless steel (reservoir)
Liquid line ($L \times ID$)	0.5 m × 2 mm	1 m × 5.3 mm
Vapor line ($L \times ID$)	0.5 m × 4 mm	1 m × 5.3 mm
Evaporator shape	Flat, rectangular	Cylindrical
Evaporator dimensions	0.05 × 0.04 m	0.6 × 0.024 m ($L \times OD$)
Porous wick material	Polypropylene	Sintered powder Ni
Wick conductivity	0.2 W/m · K	40 W/m · K
Wick porosity	0.4 to 0.5	0.6
Wick pore diameter	0.5 μm	3.2 μm
Heat input	10 to 80 W	10 to 700 W
Maximum heat flux	6.5 W/cm^2	2.2 W/cm^2
Heat sink temperature	20°C	−10 to 20°C
Ambient temperature	25°C	0 to 30°C

where T_E and T_v are the experimental temperatures of the evaporator wall and the saturated vapor, respectively. For the simulations with the LHP geometry of Boo and Chuang [8], R_E is equal to 0.34 K/W for methanol, 0.6 K/W for ethanol, and 0.45 K/W for acetone. Experimental data of the evaporation heat transfer in a nickel-cylinder wick can be found in the study of Chuang [21]. The evaporation heat transfer coefficient varies quasi-linearly from 8000 $\mathrm{W/m^2 \cdot K}$ at $Q_i = 200$ W to 15,000 $\mathrm{W/m^2 \cdot K}$ at $Q_i = 700$ W; converted into thermal resistance, R_E varies from 0.0035 K/W at 200 W to 0.002 K/W at 700 W. In the numerical simulations performed with the LHP geometry of Chuang, we used a constant value of 0.003 K/W.

The overall heat transfer in the condenser, K_C, includes the convective heat transfer between the heat sink and the condenser wall, the conductive heat transfer, and the condensation heat transfer in the smooth tubing. For such heat transfer combination, the convective thermal resistance is usually dominant. Unfortunately, in most published LHP experimental studies, heat sinks are usually not precisely described. Consequently, it is not possible to select an appropriate correlation to calculate the convective heat transfer in the heat sink. In the present model, the convective heat transfer in the heat sink is adjusted following the slope of the LHP experimental operating curve in the fixed conductance mode, whereas the condensation heat transfer is calculated using common correlations available in the open literature. Indeed, at fixed conductance mode, the slope of this curve mainly depends on the global heat transfer coefficient in the condensation area, as long as dryout does not occur in the capillary wick in the evaporator. The global heat transfer in the condenser K_C has been adjusted to 430 and 600 $\mathrm{W/m^2 \cdot K}$ for the Boo and Chung [8] and Chuang [21] studies, respectively. We calculated the overall heat transfer coefficient in the subcooled area, K_{sub}, to 220 and 230 $\mathrm{W/m^2 \cdot K}$ for the studies of Boo and Chung [8] and Chuang [21], respectively, using the same external heat transfer coefficient as in the expression of K_C and the Nusselt correlation for the convective heat transfer coefficient inside the smooth tubing.

A simple iteration loop is necessary to calculate the LHP operating temperature T because the variation of some fluid thermophysical properties with the temperature may significantly affect the results. In the following results, the LHP operating temperature T is the reservoir temperature. However, it should be noted that this temperature is close to the vapor temperature. Indeed, results from experimental or theoretical studies always show that $(T_v - T_R) \ll (T_v - T_{\mathrm{sink}})$, whatever the LHP configuration or the working fluid. Thus, the reservoir temperature calculated from our model can be compared with experimental measurements of LHP vapor temperatures available in the literature.

Figures 3–6 show the operating curves for the LHP geometry of Boo and Chung [8] at various boundary conditions. The LHP operating curves when methanol or acetone is used as the working fluid are shown in Figs. 3 and 4, respectively. The ambient and sink temperatures are equal, which means that the heat exchange between the liquid line and the ambient can be neglected. These LHP operating curves are obtained from the experimental results T_{exp}, the numerical model T_{model}, and the simplified analytical models T_{VCM} [Eq. (31)] and T_{FCM} [Eq. (37)]. The good agreement between T_{exp} and T_{model} highlights the ability of the numerical model to predict the LHP steady-state operation in various configurations. Consequently, the numerical model can be used to validate the simplified analytical model, especially for the configurations for which experimental results are not available.

In Figs. 3 and 4, a good agreement is observed between T_{model} and T_{VCM} at low heat fluxes, whatever the working fluid. The flattened shape of the LHP operating curve of VCM can be explained as follows: When considering the operating conditions used in Boo and Chung [8] nickel-cylinder study, we note the following:

1) $T_{\mathrm{sink}} = T_A$.

2) The LHP operates at horizontal position (or under microgravity environment).

3) Low-reservoir heat exchanges with the environment.

4) The low-evaporation heat transfer coefficient $T_E - T_V \gg T_v - T_R$ [Eq. (31)] may be simplified to

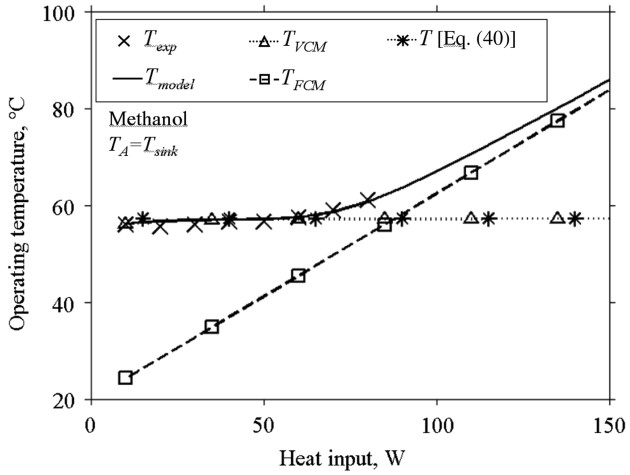

Fig. 3 Comparison between experimental and model results with methanol as the working fluid; the LHP geometry is as per Boo and Chung [8].

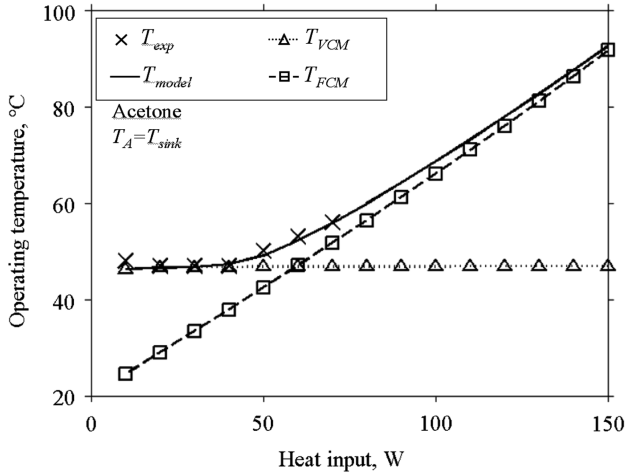

Fig. 4 Comparison between experimental and model results with acetone as the working fluid; the LHP geometry is as per Boo and Chung [8].

$$T = T_{\mathrm{sink}} + \frac{l_v}{c_{p,l}} \frac{R_E}{R_{\mathrm{wall}}} \tag{40}$$

Equation (40) clearly indicates that the LHP operating curve has a flattened shape: T does not depend on the heat flux (assuming that R_E is not sensitive to the heat flux in this mode or in the last heat-flux range). Its level depends on T_{sink}, on a fluidic term $l_v R_E / c_{p,l}$, and on a geometrical term R_E/R_{wall}. It could be noted that R_E is simultaneously a fluidic and geometrical term, because it depends on the evaporator and wick materials, on the mechanical contact between them, on the wettability of the liquid in the porous wick, and on the location of the interface. For larger heat fluxes, the FCM equation (37) seems to be the most appropriate to predict the LHP operating temperature.

In this way, the entire operating temperature profile versus the heat input may be deduced from the equation

$$T = \max(T_{\mathrm{VCM}}, T_{\mathrm{FCM}}) \tag{41}$$

The relative difference between the operating temperatures calculated from the numerical and analytical models for the LHP configurations of Figs. 3 and 4 is maximal at the transition between the variable and fixed conductance modes and does not exceed 15% of $T - T_{\mathrm{sink}}$.

The effect of the difference between the ambient and the sink temperatures on the operating temperature is shown in Fig. 5 with

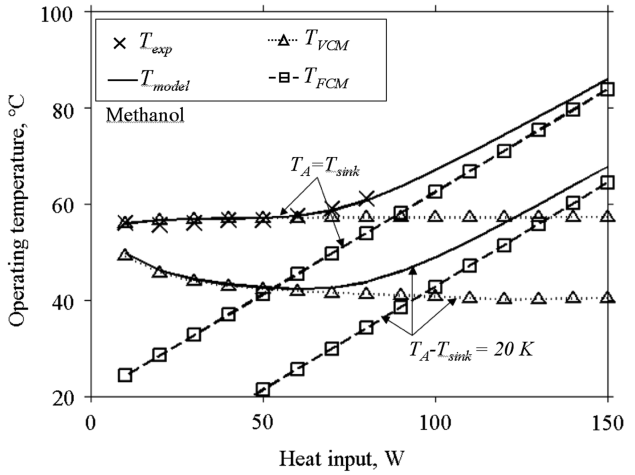

Fig. 5 Effect of the temperature difference between ambient and heat sink on T_R; the LHP geometry is as per Boo and Chung [8].

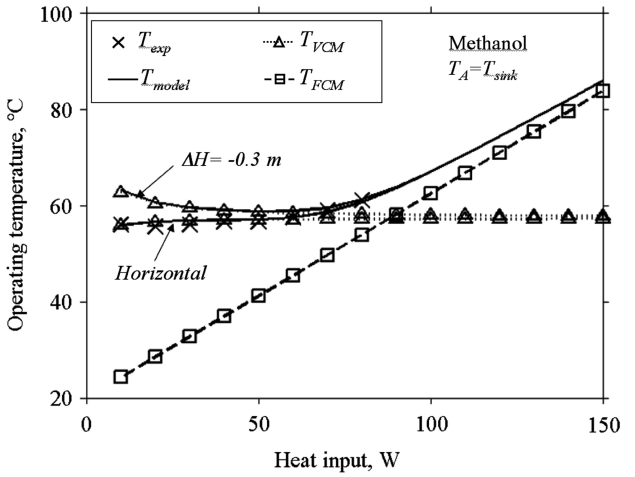

Fig. 6 Effect of the elevation on T_R; the LHP geometry is as per Boo and Chung [8].

methanol as the working fluid. As before, T_{VCM} and T_{FCM} are in good agreement with T_{model} at low and high heat input, respectively, for $T_A = T_{\mathrm{sink}}$ and $T_A - T_{\mathrm{sink}} = 20$ K. A U-shaped operating curve appears for large values of $T_A - T_{\mathrm{sink}}$ due to the large variation of liquid flow temperature caused by the heat exchange along the liquid line with the surroundings.

Compared with the numerical model, the analytical model provides additional information about the transition heat input between variable and fixed conductance modes, denoted as Q_{trans}. An approximate value of Q_{trans} is obtained by calculating the intersection point of the operating curves for VCM and FCM:

$$T_{\mathrm{VCM}} = T_{\mathrm{FCM}} \tag{42}$$

Simple analytical expressions of Q_{trans} may be determined for LHP-specific configurations. As an example, using the assumptions for the LHP configuration of Boo and Chung [8] to obtain Eq. (40), the expression of Q_{trans} becomes

$$Q_{\mathrm{trans}} \approx \frac{\pi D_C L_C \dfrac{R_E}{R_{\mathrm{ax}}}\left(1 + \dfrac{R_E}{R_{\mathrm{wall}}}\right)}{\left(\dfrac{1}{K_C} + \dfrac{R_E/R_{\mathrm{wall}}}{K_{\mathrm{sub}}}\right)} \frac{l_v}{c_{p_l}} \tag{43}$$

The simplified analytical model is also able to predict the LHP steady-state operation with respect to the LHP elevation (Fig. 6) or the LHP geometry (Fig. 7). In Fig. 6, the U-shaped curve at low heat flux is induced by the liquid hydrostatic pressure, which is large

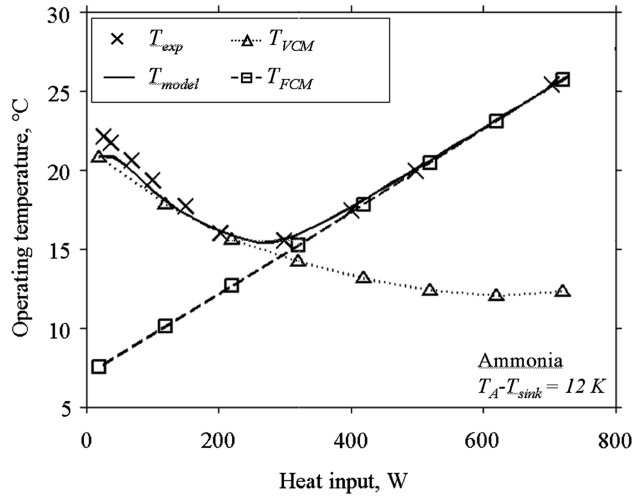

Fig. 7 Comparison between numerical and analytical results with ammonia as the working fluid; the LHP geometry is as per Chuang et al. [21,22].

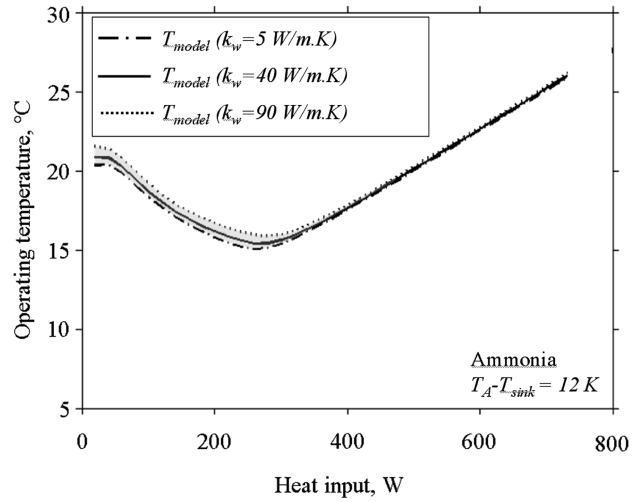

Fig. 8 Effect of the wick thermal conductivity on the operating temperature, the LHP geometry is as per Chuang et al. [21,22].

compared with the fluid viscous pressure drops. Results in Fig. 7 have been obtained for Chuang's [21] geometry (Table 1) with ammonia as the working fluid. T_A and T_{sink} are fixed at 19 and 7°C, respectively. The thermal conductivity of the sintered powder wick used in LHP tested by Chuang was not given in [21]. Dispersed values of the effective thermal conductivity of sintered powder wick have been found in the literature [18,23], ranging between 3 to 90 $\mathrm{W/m \cdot K}$. In the present study, we used an effective thermal conductivity of 40 $\mathrm{W/m \cdot K}$.

Because of the uncertainty on the wick thermal conductivity k_w, a parametric study has been performed, varying k_w from 5 to 90 $\mathrm{W/m \cdot K}$ in the numerical model (variation of the effective thermal conductivity $k_{w\mathrm{eff}}$ from 2.4 to 36 $\mathrm{W/m \cdot K}$ using volume averaging). Figure 8 shows the effect of k_w on the LHP operating temperature. Minor effects have been observed in VCM due to the distribution of the heat leak. Results indicate that the total heat leak only represents 1 to 2% of the heat input. The major part of the heat leaks by conduction through the evaporator wall; the other part, ranging between 3 and 30% of the total heat leak (function of k_w), leaks by convective–conductive heat transfer through the wick. Consequently, the liquid subcooling variation at the reservoir inlet due to k_w variation is around 1 K, which is relatively small compared with the liquid subcooling variation in the liquid line (5 to 10 K) due to heat exchange with ambient.

V. Conclusions

The present paper is related to the development of a closed-form analytical model of a LHP, based on the simplification of the equations of a steady-state numerical model, which has been described in a previous paper. This simplified model has been validated for each LHP operating mode, for various fluids (ammonia, methanol, and acetone), wick characteristics (high or low thermal conductivity), geometries (cylindrical or flat evaporator), and operating conditions (elevation of the evaporator above the condenser and temperature difference between ambient and heat sink). The simplified model also gives closed-form equations of the LHP operating temperature and the heat-flux value at the transition between variable and fixed conductance modes. The relative difference between the global and analytical models is maximum at the transition between the variable and fixed conductance modes, but it does not exceed 15%. We believe that this model could be a useful tool for the design of LHPs, because the effect of geometrical parameters and fluid thermophysical properties on the LHP performance can be clearly and easily highlighted analytically.

In the present state, most of the input data of the analytical model can be easily estimated from the LHP geometry, the fluid properties, and the operating conditions, except the evaporator thermal resistance R_E. Thus, an identification of this parameter is required by adjusting the model results to experimental data. The LHP analytical model could be further improved by introducing a correlation for the calculation of R_E. Another improvement of our model would be to extend its application to a wider range of operating conditions. For instance, the model could be further developed to predict the LHP behavior when the reservoir is entirely filled with liquid.

Acknowledgments

This work was conducted in the frame of the European Project COSEE (Cooling of Seat Electronic Box and Cabin Equipment), funded by the European Commission (contract no. AST5-CT-2006-030800). The authors are very grateful to Sameer Khandekar (Indian Institute of Technnology, Kanpur, India) for his fruitful comments made during his stay at Institut National des Sciences Appliquées de Lyon as a Visiting Professor.

References

[1] Orlov, A. A., Goncharov, K. A., Kotliarov, E., Tyklina, T. A., Ustinov, S. N., and Maidanik, Y. F., "The Loop Heat Pipe Experiment on Board the 'GRANAT' Spacecraft," *Sixth European Symposium on Space Environmental Control Systems*, SP400, ESA, Noordwijk, The Netherlands, 1997, pp. 341–353.

[2] Grob, E., Baker, C., and McCarthy, T., "In-Flight Thermal Performance of the Geoscience Laser Altimeter System (GLAS) Instrument," 33rd International Conference on Environmental Systems, Society of Automotive Engineers Paper 2003-01-2421, July 2003.

[3] Pastukhov, V. G., Maidanik, Y. F., Vershinin, C. V., and Korukov, M. A., "Miniature Loop Heat Pipes for Electronics Cooling," *Applied Thermal Engineering*, Vol. 23, No. 9, 2003, pp. 1125–1135. doi:10.1016/S1359-4311(03)00046-2

[4] Maydanik, Y. F., "Miniature Loop Heat Pipe," *Proceedings of the 13th International Heat Pipe Conference*, 21–25 Sept. 2004, pp. 23–35.

[5] Maidanik, Y. F., "Loop Heat Pipes," *Applied Thermal Engineering*, Vol. 25, Nos. 5–6, 2005, pp. 635–657. doi:10.1016/j.applthermaleng.2004.07.010

[6] Launay, S., Sartre, V., and Bonjour, J., "Parametric Analysis of Loop Heat Pipe Operation: A Literature Review," *International Journal of Thermal Sciences*, Vol. 46, No. 7, 2007, pp. 621–636. doi:10.1016/j.ijthermalsci.2006.11.007

[7] Chen, Y., Groll, M., Mertz, R., Maydanik, Y. F., and Vershinin, S. V., "Steady-State and Transient Performance of a Miniature Loop Heat Pipe," *International Journal of Thermal Sciences*, Vol. 45, No. 11, 2006, pp. 1084–1090. doi:10.1016/j.ijthermalsci.2006.02.003

[8] Boo, J. H., and Chung, W. B., "Thermal Performance of a Small-Scale Loop Heat Pipe with PP Wick," *Proceedings of the 13th International Heat Pipe Conference*, Sept. 2004, pp. 259–264.

[9] Riehl, R. R., and Siqueira, T., "Heat Transport Capability and Compensation Chamber Influence in Loop Heat Pipes Performance," *Applied Thermal Engineering*, Vol. 26, Nos. 11–12, 2006, pp. 1158–1168. doi:10.1016/j.applthermaleng.2005.10.037

[10] Ku, J., "Operating Characteristics of Loop Heat Pipes," Society of Automotive Engineers Paper 1999-01-2007, July 1999.

[11] Borodkin, A. A., Sasin, V. Ya., Kotliarov, E.Yu., and Goncharov, K. A., "Loop Heat Pipes Heat Transfer Characteristics Analysis by Using Monograms," 26th International Conference on Environmental Systems, Society of Automotive Engineers Paper 961566, July 1996.

[12] Kaya, T., and Hoang, T. T., "Mathematical Modeling of Loop Heat Pipes and Experimental Validation," *Journal of Thermophysics and Heat Transfer*, Vol. 13, No. 3, 1999, pp. 314–320.

[13] Kaya, T., and Ku, J., "Thermal Operational Characteristics of a Small Loop Heat Pipe," *Journal of Thermophysics and Heat Transfer*, Vol. 17, No. 4, 2003, pp. 464–470.

[14] Hamdan, M., Gerner, F. M., and Henderson, H. T., "Steady-State Model of a Loop Heat Pipe (LHP) with Coherent Porous Silicon (CPS) Wick in the Evaporator," *19th Annual IEEE Semiconductor Thermal Measurement and Management Symposium*, Inst. of Electrical and Electronics Engineers, Piscataway, NJ, 11–13 Mar. 2003, pp. 88–96.

[15] Hoang, T. T., and Kaya, T., "Mathematical Modeling of Loop Heat Pipes with Two-Phase Pressure Drop," 33rd AIAA Thermophysics Conference, Norfolk, VA, AIAA Paper 99-3448, 1999.

[16] Maydanik, Y. F., Fershtater, Y. G., and Solodovnik, N., "Loop Heat Pipes: Design, Investigation, Prospects of Use in Aerospace Technics," Society of Automotive Engineers Paper 941185, 1994.

[17] Furukawa, M., "Model-Based Method of Theoretical Design Analysis of a Loop Heat Pipe," *Journal of Thermophysics and Heat Transfer*, Vol. 20, No. 1, 2006, pp. 111–121. doi:10.2514/1.14675

[18] Mo, S., Hu, P., Cao, J., Chen, Z., Fan, H., and Yu, F., "Effective Thermal Conductivity of Moist Porous Sintered Nickel Material," *International Journal of Thermophysics*, Vol. 27, No. 1, 2006, pp. 304–313. doi:10.1007/s10765-006-0030-9

[19] Bejan, A., and Krauss, A. D., *Heat Transfer Handbook*, Wiley, New York, 2003, p. 1480.

[20] Launay, S., Sartre, V., and Bonjour, J., "Effect of Fluid Thermophysical Properties on Loop Heat Pipe Operation," *Proceedings of the 14th International Heat Pipe Conference*, Apr. 2007, p. 6.

[21] Chuang, P-Y. A., "An Improved Steady-State Model of Loop Heat Pipes Based on Experimental and Theoretical Analyses," Ph.D. Dissertation, Pennsylvania State Univ., State College, PA, 2003.

[22] Chuang, P-Y. A., Cimbala, J. M., Brenizer, J. S., Conroy, C. T., El-Ganayni, A. A., and Riley, R. D., "Comparison of Experiments and 1-D Steady-State Model of a Loop Heat Pipe," International Mechanical Engineering Congress and Exposition, American Society of Mechanical Engineers Paper IMECE 2002-33542, Nov. 2002.

[23] Wan, Z., Liu, W., Zheng, Z., and Nakayama, A., "Heat Transfer with Flow and Phase Change in an Evaporator of Miniature Flat Plate Capillary Pumped Loop," *Journal of Thermal Science*, Vol. 16, No. 3, 2007, pp. 254–263. doi:10.1007/s11630-007-0254-4